

## RESEARCH ARTICLE

# Longitudinal trajectory of Amyloid-related hippocampal subfield atrophy in nondemented elderly

Liwen Zhang<sup>1,3,4</sup> | Elijah Mak<sup>6</sup> | Anthonin Reilhac<sup>5</sup> | Hee Y. Shim<sup>1,3</sup> |  
 Kwun K. Ng<sup>2,3</sup> | Marcus Q. W. Ong<sup>2,3</sup> | Fang Ji<sup>2,3</sup> | Eddie J. Y. Chong<sup>1,4</sup> |  
 Xin Xu<sup>1,4</sup> | Zi X. Wong<sup>1,4</sup> | Mary C. Stephenson<sup>5</sup> |  
 Narayanaswamy Venketasubramanian<sup>7</sup> | Boon Y. Tan<sup>8</sup> | John T. O'Brien<sup>6</sup> |  
 Juan H. Zhou<sup>2,3,5</sup>  | Christopher L.H. Chen<sup>1,4</sup> the Alzheimer's Disease Neuroimaging Initiative

<sup>1</sup>Department of Pharmacology, Yong Loo Lin School of Medicine, National University of Singapore, Singapore, Singapore

<sup>2</sup>Center for Sleep and Cognition, Department of Medicine, Yong Loo Lin School of Medicine, National University of Singapore, Singapore

<sup>3</sup>Center for Cognitive Neuroscience, Neuroscience and Behavioural Disorders Program, Duke-National University of Singapore Medical School, Singapore

<sup>4</sup>Memory Ageing and Cognition Centre, National University Health System, Singapore, Singapore

<sup>5</sup>Clinical Imaging Research Center, Yong Loo Lin School of Medicine, National University Health System, Singapore, Singapore

<sup>6</sup>Department of Psychiatry, University of Cambridge, Cambridge, United Kingdom

<sup>7</sup>Raffles Neuroscience Centre, Raffles Hospital, Singapore, Singapore

<sup>8</sup>St. Luke's Hospital, Singapore, Singapore

## Correspondence

Juan H. Zhou, Center for Sleep and Cognition, Yong Loo Lin School of Medicine, Tahir Foundation Building (MD1), 12 Science Drive 2, #13-05, National University of Singapore, Singapore 117549, Singapore.  
 Email: helen.zhou@nus.edu.sg

Christopher L.-H. Chen, Department of Pharmacology, Yong Loo Lin School of Medicine, National University of Singapore, 16 Medical Dr, Block MD3, Level 4, #04-01, Singapore 117600, Singapore.  
 Email: phccclh@nus.edu.sg

## Funding information

Biomedical Research Council Singapore, Grant/Award Number: BMRC 04/1/36/372; Cambridge-NUHS Seed Funding, Grant/Award Number: NUHSRO/2017/014/Cambridge/01; Duke-NUS Medical School Signature Research Program; National Institute for Health Research Cambridge Biomedical Research

## Abstract

Hippocampal atrophy and abnormal  $\beta$ -Amyloid ( $A\beta$ ) deposition are established markers of Alzheimer's disease (AD). Nonetheless, longitudinal trajectory of  $A\beta$ -associated hippocampal subfield atrophy prior to dementia remains unclear. We hypothesized that elevated  $A\beta$  correlated with longitudinal subfield atrophy selectively in no cognitive impairment (NCI), spreading to other subfields in mild cognitive impairment (MCI). We analyzed data from two independent longitudinal cohorts of nondemented elderly, including global PET- $A\beta$  in AD-vulnerable cortical regions and longitudinal subfield volumes quantified with a novel auto-segmentation method (FreeSurfer v.6.0). Moreover, we investigated associations of  $A\beta$ -related progressive subfield atrophy with memory decline. Across both datasets, we found a converging pattern that higher  $A\beta$  correlated with faster CA1 volume decline in NCI. This pattern spread to other hippocampal subfields in MCI group, correlating with memory decline. Our results for the first time suggest a longitudinal focal-to-widespread trajectory of  $A\beta$ -associated hippocampal subfield atrophy over disease progression in nondemented elderly.

Data used in preparation of this article were obtained from the Alzheimer's Disease Neuroimaging Initiative (ADNI) database (adni.loni.usc.edu). As such, the investigators within the ADNI contributed to the design and implementation of ADNI and/or provided data but did not participate in analysis or writing of this report. A complete listing of ADNI investigators can be found at: [http://adni.loni.usc.edu/wp-content/uploads/how\\_to\\_apply/ADNI\\_Acknowledgement\\_List.pdf](http://adni.loni.usc.edu/wp-content/uploads/how_to_apply/ADNI_Acknowledgement_List.pdf)

This is an open access article under the terms of the Creative Commons Attribution-NonCommercial License, which permits use, distribution and reproduction in any medium, provided the original work is properly cited and is not used for commercial purposes.

© 2020 The Authors. *Human Brain Mapping* published by Wiley Periodicals, Inc.

Centre; Center grant, collaborative basic-scientist individual research grant and clinical individual research grant, Grant/Award Numbers: NMRC/CBRG/0088/2015, NMRC/CG/013/2013, NMRC/CG/NUHS/2010, NMRC/CIRG/1390/2014, NMRC/CIRG/1446/2016

## KEYWORDS

hippocampal subfield atrophy, longitudinal atrophy trajectory, nondemented elderly,  $\beta$ -Amyloid

## 1 | INTRODUCTION

Hippocampal atrophy and abnormal  $\beta$ -Amyloid ( $A\beta$ ) are characteristic of Alzheimer's disease (AD; Barnes et al., 2009; Jack Jr. et al., 2013). Evidence from animal models suggest that  $A\beta$  burden may affect hippocampal neurodegeneration via synaptic or neuronal dysfunctions (Busche et al., 2012; Busche & Konnerth, 2015; Masters, Cappai, Barnham, & Villemagne, 2006; Perez-Cruz et al., 2011). Indeed, greater PET- $A\beta$  burden was associated with smaller volume cross-sectionally (Chetelat et al., 2013; Hanseeuw, Dricot, Lhomme, Quenon, & Ivanoiu, 2016; Mormino et al., 2009) and faster volume decline longitudinally in the whole hippocampus (Villemagne et al., 2013) in nondemented elderly. Nevertheless, lack of association between PET- $A\beta$  and whole hippocampal atrophy was also found in cognitively normal elderly (Becker et al., 2011). Given  $A\beta$ -associated hippocampal atrophy in nondemented elderly but not in patients with AD-dementia (Chetelat et al., 2010), it may be implied that  $A\beta$  affects hippocampal degeneration more robustly in early disease stage while other pathologies contribute more in dementia stage. This is in line with the AD Pathological Cascade model (Jack Jr. et al., 2013) proposing that  $A\beta$  accumulation precedes hippocampal atrophy and both reach a plateau at dementia or earlier. Nonetheless, the longitudinal trajectory of  $A\beta$ -associated hippocampal atrophy in predementia remains unclear.

Notably, the hippocampus consists of several subfields (Bakker, Kirwan, Miller, & Stark, 2008; Small, Schobel, Buxton, Witter, & Barnes, 2011). A review concluded selective subfield atrophy before dementia, more consistently in the CA1/subiculum (de Flores, La Joie, & Chetelat, 2015). Few studies tested  $A\beta$ -associated subfield atrophy in nondemented elderly, showing smaller subiculum/hippocampal-tail/presubiculum in  $A\beta$ -positive no cognitive impairment (NCI; vs.  $A\beta$ -negative NCI) (Hsu et al., 2015), and smaller CA1/subiculum in  $A\beta$ -positive mild cognitive impairment (MCI) compared with NCI (but no difference compared with  $A\beta$ -negative MCI) (La Joie et al., 2013). These findings suggest selective hippocampal subfield atrophy related to  $A\beta$  in predementia.

However, previous studies relied on manual segmentation (La Joie et al., 2013) or earlier in-vivo atlas-based FreeSurfer approach (Hsu et al., 2015), leading to hippocampal segmentation inaccuracy (Iglesias et al., 2015; Wisse, Biessels, & Geerlings, 2014). Moreover, cross-sectional design and dichotomized  $A\beta$ -status prevented them from testing longitudinal trajectories of  $A\beta$ -associated subfield atrophy accurately.

Therefore, we aimed to investigate how  $A\beta$  influence hippocampal-subfield atrophy in NCI/MCI longitudinally in two independent datasets, applying a novel ex-vivo ultra-high-resolution atlas-based automatic hippocampal segmentation (FreeSurfer v.6.0). We hypothesized  $A\beta$ -associated longitudinal atrophy in selective subfields (e.g., CA1/

subiculum), spreading to other subfields over disease deterioration in nondemented elderly. Furthermore, we tested whether  $A\beta$ -associated progressive subfield atrophy correlated with memory decline.

## 2 | METHODS

### 2.1 | Participants

This study recruited participants from two independent datasets: (a) 75 NCI and 104 MCI who were new patients from the Alzheimer's Disease Neuroimaging Initiative (ADNI2) study as defined on July 10, 2018 and (b) 20 NCI and 93 MCI from Memory Aging and Cognition Centre (MACC) dataset recruited from memory clinics/community in Singapore (Chong et al., 2017). ADNI data were obtained from the ADNI database (<http://adni.loni.usc.edu/>). ADNI is a public-private partnership (PI: Dr. Michael W. Weiner), testing whether MRI, PET, clinical/neuropsychological assessment, and other biological markers can be combined to measure the progression of MCI and early AD.

For the MACC dataset, weekly consensus meetings were organized between neurologists, psychologists, and research personnel to make diagnosis based on clinical observations, CT and/or MRI scans, and laboratory tests. Diagnosis of MCI was made if patients had subjective cognitive complaint and objective impairment in at least one domain on the locally validated neuropsychological assessment battery (see Section 2.2), but remained functionally independent and not demented. For MACC participants, exclusion criteria included: (a) comorbidity with neuropsychiatric disorders (e.g., bipolar disorder) or epilepsy associated with cognitive impairment; (b) disorders that may influence the central nervous system (e.g., current or past substance abuse disorder, nutritional, toxic, or traumatic disorder) in accordance with the Diagnostic and Statistical Manual of Mental Disorders (DSM-IV); (c) central nervous system infections, such as bacterium, Creutzfeldt-Jacob disease, viral encephalitis, fungi, syphilis, tuberculosis, or rickettsiae; (d) hypo-/hyper-tensive, hypoxic/anoxic, uremic, or hepatic encephalopathy; (e) intracerebral hemorrhage possibly leading to impaired cognition; (f) space occupying intracranial lesion (e.g., tumor); (g) inflammatory vasculitides, cranial arteritis, or moyamoya disease in the central nervous system; (h) normal or obstructive pressure hydrocephalus; (i) cortical infarct leading to surface model reconstruction errors. Moreover, the following exclusion criteria were applied for both datasets, including (a) MRI-incompatibilities (e.g., mental implants, pregnancy); (b) surface model reconstruction errors for structural images (see MRI preprocessing); (c) NCI participants with a score of <26 on the Mini-Mental State Examination (MMSE).

After image quality control (see Section 2.4), 52 NCI and 77 MCI from the ADNI were included in the final cross-sectional and

**TABLE 1** Demographic and neuropsychological features of participants included in the cross-sectional analysis of the ADNI dataset and MACC dataset

|                                       | ADNI dataset    |                 |             |        | MACC dataset    |                 |             |        |
|---------------------------------------|-----------------|-----------------|-------------|--------|-----------------|-----------------|-------------|--------|
|                                       | NCI<br>(n = 52) | MCI<br>(n = 77) | t/ $\chi^2$ | p      | NCI<br>(n = 15) | MCI<br>(n = 76) | t/ $\chi^2$ | p      |
| Age, M(SD) <sup>f</sup>               | 73.7 (6.7)      | 68.6 (6.5)      | 4.40        | <.001* | 73.2 (7.4)      | 76.0 (5.9)      | 1.59        | .12    |
| Male/female                           | 24/28           | 35/42           | 0.006       | .94    | 8/7             | 37/39           | 0.11        | .74    |
| Handedness, R/L <sup>f</sup>          | 46/6            | 68/9            | 0.001       | .98    | 15/0            | 74/2            | 0.40        | .53    |
| Ethnicity, H,L/non-H,L or C/non-C     | 2/50            | 0/77            | 3.01        | .08    | 15/0            | 65/11           | 2.47        | .12    |
| Education, M (SD) <sup>e,f</sup>      | 16.9 (2.4)      | 16.5 (2.6)      | 0.85        | .40    | 8.0 (4.8)       | 8.6 (4.7)       | 0.41        | .68    |
| CDR-SOB, M (SD) <sup>a,f</sup>        | 0.02 (0.1)      | 1.3 (0.9)       | 12.16       | <.001* | 0.0 (0.0)       | 0.8 (0.9)       | 7.39        | <.001* |
| MMSE, M (SD) <sup>a, f</sup>          | 29.3 (1.1)      | 28.3 (1.6)      | 4.37        | <.001* | 28.6 (1.2)      | 24.4 (3.6)      | 7.17        | .001*  |
| A $\beta$ burden, M (SD) <sup>b</sup> | 0.11 (0.4)      | 0.24 (0.4)      | 1.61        | .11    | 0.12 (0.3)      | 0.40 (0.5)      | 2.88        | .007*  |
| A $\beta$ burden, range <sup>b</sup>  | -0.4~1.1        | -0.4~1.1        | -           | -      | -0.2~0.9        | -0.2~1.6        | -           | -      |
| WMH burden, M (SD) <sup>b</sup>       | 0.94 (1.3)      | 0.81 (1.1)      | 0.61        | .55    | 1.6 (2.3)       | 1.8 (1.8)       | 0.34        | .73    |
| Dementia convertor, no. (%)           | 0 (0)           | 17 (22.1)       | -           | -      | 0 (0)           | 3 (4.0)         | -           | -      |
| Remitter, no. <sup>c</sup> (%)        | 0 (0)           | 0 (0)           | -           | -      | 0 (0)           | 1 (1.3)         | -           | -      |
| Follow-up months, M (SD) <sup>d</sup> | 48.4 (6.9)      | 46.3 (8.2)      | 1.58        | .118   | 23.3 (1.8)      | 23.7 (2.0)      | 0.59        | .556   |

Note: All NCI included in the present study had a MMSE score of  $\geq 26$ . Groups were compared within each dataset or between datasets on the listed variables, using independent-samples T test or chi-square tests where appropriate, with a threshold of  $p < .05$  (\*, two-tailed). We did not compare A $\beta$ , WMH, and ethnicity between datasets due to difference in radiotracer, WMH quantification method and recruited population, respectively.

Abbreviations: C/non-C, Chinese/non-Chinese; CDR-SOB, Clinical Dementia Rating Sum of Boxes score; H,L/non-H,L, Hispanic or Latino/non-Hispanic or Latino; L, left; M, mean; MCI, mild cognitive impairment; MMSE, Mini-Mental State Examination; N, number; NCI, no cognitive impairment; R, right; SD, standard deviation; WMH, white matter hyperintensity.

<sup>a</sup>Six NCI did not have MMSE and CDR-SOB scores, and CDR-SOB score was not available for two MCI from the MACC dataset.

<sup>b</sup>A $\beta$  and WMH represented log-transformed SUVR score with PVC and log-transformed WMH volume respectively.

<sup>c</sup>This participant remitted from dementia (baseline) to NCI (Year 2), and then deteriorated to MCI during subsequent PET scanning, based on which we included this participant in cross-sectional analyses but excluded from the longitudinal investigation.

<sup>d</sup>For MACC dataset, a subset of 12 NCI and 45 MCI were included in the longitudinal analyses.

<sup>e</sup>We compared the same group between datasets, with significance being indicated for NCI.

<sup>f</sup>We compared the same group between datasets, with significance being indicated for MCI.

longitudinal analyses with annual follow-ups up to 4-years (Table 1). For the MACC dataset, 15 NCI and 76 MCI were included in the cross-sectional analyses. A subset of 12 NCI and 45 MCI who had two MRI scans were selected for the longitudinal analyses (Table 1; see Section 2.3 for MACC selection note). There was no difference in follow-up time between NCI and MCI for both datasets, although the follow-up time was in general shorter in the MACC dataset compared with the ADNI dataset (Table 1).

This study was conducted in line with the Helsinki Declaration, and the MACC study was approved by the National Healthcare Group Domain-Specific Review Board and SingHealth Institutional Review Board. All participants have provided written consent.

## 2.2 | Neuropsychological assessments

In both datasets, the MMSE and Clinical Dementia Rating (CDR) were performed. Regarding the MACC dataset, a locally validated neuropsychological assessment battery was administered to all participants, including two memory domains (verbal and visual memory), and five nonmemory domains (language, attention, executive function, visuoconstruction, and visuomotor speed) following our previous

work (Ji et al., 2017; Vipin et al., 2018). Standardized z-score for each domain was calculated following previous publication (Xu et al., 2015). A memory z-score was calculated by averaging the z-scores between the two memory domains for MACC. For ADNI, we used the ADNI memory z-score as validated by previous work (Crane et al., 2012).

## 2.3 | Image acquisition

For both datasets, whole-brain T1-weighted structural MRI images were collected using the Magnetization prepared rapid gradient recalled echo (MPRAGE) sequence. ADNI participants were scanned in a 3T scanner (SIEMENS Magnetom Tim Trio, Skyra and Verio scanner, or PHILIPS Magnetom Achieva, Intera, and Ingenia scanner depending on the scanning site) at baseline and annual follow-up (176 sagittal slices, voxel size =  $1 \times 1 \times 1.2$  mm<sup>3</sup>, TR/TE/TI = 2300/2.98/900 ms, FOV =  $240 \times 256$  mm<sup>2</sup>, flip angle = 9°). MACC participants were scanned in a 3T Siemens Magnetom Tim Trio scanner (32-channel head coil) at baseline and Year 2 (192 sagittal slices, voxel size =  $1 \times 1 \times 1$  mm<sup>3</sup>, TR/TE/TI = 2300/1.9/900 ms, FOV =  $256 \times 256$  mm<sup>2</sup>, flip angle = 9°). The MACC MRI scanning protocol also included a Fluid attenuation inversion recover (FLAIR) image (48 axial slices, voxel

size =  $1 \times 1 \times 3 \text{ mm}^3$ , TR/TE/TI = 9000/82/2500 ms, flip angle =  $180^\circ$ , FOV =  $232 \times 256 \text{ mm}^2$ ).

The PET emission protocols were as follows: (a) ADNI dataset: 370 MBq  $^{18}\text{F}$ -AV-45 injection was followed by dynamic imaging (four 5-min frames) from 50 to 70 min postinjection, and PET scan was performed within 28 days from the baseline MRI scan. Other scanning parameters depended on the scanner used at different sites, as described on the ADNI website (ADNI, 2011); (b) MACC dataset: PET scanning was performed on a Siemens Biograph mMR scanner (Delso et al., 2011) at the Clinical Imaging Research Centre (National University of Singapore, Singapore), 370 MBq  $^{11}\text{C}$ -PIB injection was followed by static data acquisition from 40 to 70 min post injection (176 axial slices, voxel size =  $1 \times 1 \times 3 \text{ mm}^3$ , FOV =  $256 \times 256 \text{ mm}^2$ ). For MACC dataset, PET data were acquired per participant once during the whole longitudinal project. Therefore, we selected the MRI scan closest in time to the PET scan for the cross-sectional analysis (not necessarily baseline MRI scan, mean  $\pm$  SD:  $3.1 \pm 7.3$  months). Given the slow A $\beta$  accumulation (Villemagne et al., 2013) and for the purpose of increasing sample size for longitudinal analyses, baseline and Year 2 MRI scans were included in the MACC longitudinal analyses irrespective of PET scan time (baseline MRI-PET interval [mean  $\pm$  SD]:  $33.1 \pm 14.7$  months).

## 2.4 | Data preprocessing

### 2.4.1 | MRI preprocessing

Structural images were first checked for motion via visual inspection, and then preprocessed using the FreeSurfer pipeline (v.6.0) (Fischl et al., 2002; Fischl et al., 2004; Reuter, Schmansky, Rosas, & Fischl, 2012). The longitudinal data were further preprocessed with the standard longitudinal FreeSurfer pipeline, creating an unbiased subject-specific template for re-processing structural image at each time point. This longitudinal pipeline has shown to reduce within-subject variability and improve sensitivity to detect subtle changes (Reuter, Rosas, & Fischl, 2010). Manual editing on structural images was applied where appropriate blinded to diagnoses. Participants with surface reconstruction errors that cannot be addressed by manual editing were excluded.

### 2.4.2 | PET preprocessing

We downloaded from the ADNI website the mean aligned PET images (native space) for further preprocessing (<http://adni.loni.usc.edu/methods/pet-analysis-method/pet-analysis/> n.d.). Briefly, the four 5-min frame images were aligned to the first one and then averaged across the emission frames using the Statistical Parametric Mapping (SPM5). The MRI FreeSurfer parcellations (MRI preprocessing) were used to define the regions of interest (ROI) for subsequent calculation of standardized uptake value ratio (SUVR) from PetSurfer (Greve et al., 2016). Specifically, a high-resolution segmentation was created based

on the preprocessed structural image per participant, followed by coregistering the mean aligned PET image to the high-resolution T1-MPRAGE segmentation. Afterward, partial volume correction (PVC) was applied using the symmetric geometric transfer matrix, and SUVR scores were derived for each ROI from the FreeSurfer-defined parcellation (cerebellar gray matter as the reference region). Finally, a global SUVR score was calculated by extracting means from four main cortical regions (i.e., frontal, cingulate cortex, lateral temporal, and lateral parietal) as used in previous literature (Landau & Jagust, 2015). A global SUVR score without applying PVC was also obtained.

For MACC PET data, motion correction was performed prior to tomographic reconstruction into a single static frame, using an in-house developed rebinner with rigid motion correction, binning into 20s frames (Reilhac et al., 2018). Motion corrected images were reconstructed into a volume of  $344 \times 344 \times 344$  voxels (voxel size =  $2.09 \times 2.09 \times 2.03 \text{ mm}^3$ ) using 3D Ordinary Poisson Ordered-subsets Expectation Maximization algorithm (Panin, Kehren, Michel, & Casey, 2006) with all corrections performed (including resolution modeling) and using three iterations and 21 subsets. Subsequently, same PetSurfer based preprocessing steps were applied as used for the ADNI dataset to obtain the global SUVR score, both with and without PVC. We used the global SUVR score for subsequent statistical analyses.

## 2.5 | Hippocampal subfield segmentation

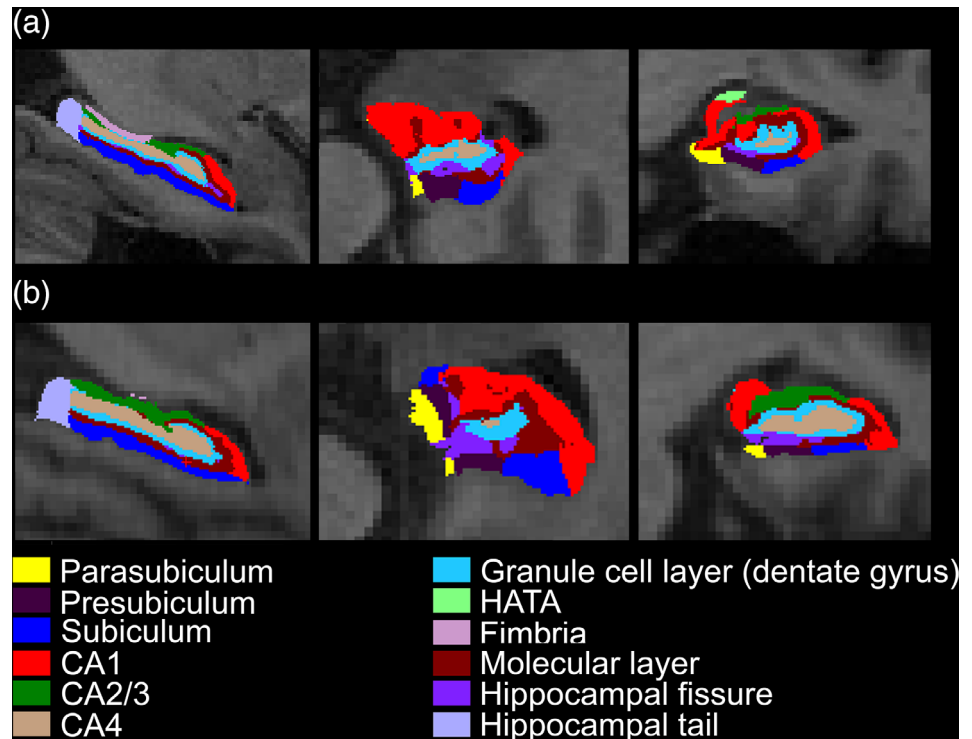
Based on the preprocessed structural-images, a subject-specific atlas based longitudinal pipeline of automated hippocampal subfield segmentation (FreeSurfer v.6.0) was used to generate more sensitive subfield volume (Iglesias et al., 2016). Since not all MACC baseline structural-images were used for longitudinal investigation (see Section 2.3), cross-sectional pipeline of hippocampal subfield segmentation (FreeSurfer v.6.0) (Iglesias et al., 2015) was applied for the MACC cross-sectional analysis, which was similar to the longitudinal pipeline without creating a subject-specific template. Importantly, both algorithms were based on a probabilistic atlas acquired from ultra-high resolution ( $\sim 0.1 \text{ mm}$ ) ex vivo MRI data, showing significantly improved segmentation accuracy compared with previous method based on in vivo atlas from the earlier FreeSurfer v.5.3, and better alignment with previous histological studies (Iglesias et al., 2015; Iglesias et al., 2016). Twelve subfields were obtained (Figure 1), and we focused on the seven gray-matter subfields following previous studies (Ho et al., 2017), including the granule cell layer of dentate gyrus (GCL), CA1, CA2/3, CA4, molecular layer (ML), hippocampal tail, and subiculum. Bilateral volume was averaged per subfield for subsequent analyses.

## 2.6 | Statistical analyses

### 2.6.1 | Longitudinal analyses

Linear mixed model (LMM) analyses (R software, v.3.5.1) were conducted to test global A $\beta$ -associated progressive hippocampal atrophy in NCI and MCI separately (Model 1). To provide a reference for any

**FIGURE 1** Exemplar illustration of hippocampal subfield segmentation based on FreeSurfer (v.6.0) in a representative NCI. One representative NCI was selected from (a) ADNI dataset and (b) MACC dataset each. The planes of sagittal (left), axial (middle), and coronal (right) are shown. Abbreviations: NCI, no cognitive impairment



observed  $A\beta$ -associated effects, we also explored the time effects only on hippocampal subfield atrophy in groups separately (Model 2).

$$\text{Volume}_{ij} = \beta_0 + \beta_1 * A\beta_i + \beta_2 * \text{Time}_{ij} + \beta_3 * A\beta_i * \text{Time}_{ij} + \beta_4 * \text{Age}_i + \beta_5 * \text{TIV}_i + b_{0i} + b_{1i} * \text{Time}_{ij} + \varepsilon_{ij} \text{ (Model 1)}$$

$$\text{Volume}_{ij} = \beta_0 + \beta_1 * \text{Time}_{ij} + \beta_2 * \text{Age}_i + \beta_3 * \text{TIV}_i + b_{0i} + b_{1i} * \text{Time}_{ij} + \varepsilon_{ij} \text{ (Model 2)}$$

where  $\text{Volume}_{ij}$  represented volume of individual subfield or whole hippocampus at time  $j$  for participant  $i$ ,  $A\beta$  was indexed with the log-transformed SUVR score, and time was the interval from baseline MRI for each time point (in month, baseline = 0). Baseline age and total intracranial volume (TIV) were added as covariates.  $\beta$  represented estimates for the fixed effects (i.e.,  $A\beta$ , Time, Age, TIV, and the interaction), and individual intercept and slope of time were modeled as subject specific random effects such that participants could have different baseline measures and longitudinal changes (estimates denoted by  $b$ ).

The MACC dataset included participants with varying cerebrovascular disease markers (e.g., cortical infarct, lacune, white matter hyperintensity [WMH], and microbleed) while ADNI dataset excluded those with significant neurologic conditions (e.g., multiple infarcts, lacunes) and had low level of WMH (Weiner et al., 2017). As such, ADNI MCI possibly had a more pure AD pathology than MACC MCI who more suffered from mixed pathology, potentially leading to different extents of atrophy progression. To test this possibility, we derived a subsample of MCI patients that were close in the WMH volume between the two datasets and repeated the analyses (Supporting Information). We did not match WMH on NCI, due to limited MACC NCI sample.

Moreover, we performed validation analyses by further controlling for age and sex, PET-MRI interval, excluding dementia converters (ADNI: 17 MCI converted to AD; MACC: three MCI converted to AD) and repeating analyses using global SUVR without PVC. To facilitate results comparison between the two datasets, we also repeated the analysis for the ADNI dataset with the first 2-year follow-up data.

For all analyses, age and TIV were included as covariates, and statistical threshold was set at  $p \leq .05$ . We applied Holm-Bonferroni multiple comparison correction for the number of subfields ( $n = 7$ ).

## 2.6.2 | Cross-sectional analyses

To provide more complete information, we also built separate cross-sectional general linear regression models for each subfield and whole hippocampus in NCI and MCI groups, with global  $A\beta$  (log-transformed SUVR) as the predictor and hippocampal volume of interest as the dependent variable.

Due to the MACC MRI scan selection (see Section 2.3), we repeated the cross-sectional analyses in NCI and MCI separately using the baseline MRI scan. Additionally, as a sanity check, we compared hippocampal subfield volume between NCI and MCI groups cross-sectionally.

## 2.6.3 | Associations between progressive hippocampal subfield atrophy and memory decline

We first built LMMs to examine whether there was memory decline over time (Model 3). For subfields showing global  $A\beta$ -associated

progressive atrophy, we investigated whether their longitudinal atrophy related to memory decline, using separate LMMs (Model 4). Analyses were performed in NCI and MCI separately. We controlled for age and TIV. Threshold was set at  $p \leq .05$ , and we applied Holm-Bonferroni multiple comparison correction for the number of subfields showing longitudinal associations with  $A\beta$ .

$$\text{Memory}_{ij} = \beta_0 + \beta_1 * \text{Time}_{ij} + \beta_2 \text{Age}_i + \beta_3 * \text{TIV}_i + b_0_i + b_1_i \text{Time}_{ij} + \epsilon_{ij} \text{ (Model 3)}$$

$$\begin{aligned} \text{Memory}_{ij} = & \beta_0 + \beta_1 * \text{volume}_{ij} + \beta_2 * \text{Time}_{ij} + \beta_3 * \text{Volume}_{ij} * \text{Time}_{ij} \\ & + \beta_4 \text{Age}_i + \beta_5 * \text{TIV}_i + b_0_i + b_1_i \text{Time}_{ij} + \epsilon_{ij} \text{ (Model 4)} \end{aligned}$$

where  $\text{Memory}_{ij}$  was the memory z-score at time  $j$  for participant  $i$ , and  $\text{volume}_{ij}$  represented individual subfield volume of interest. Denotations were the same for other parameters as stated for model 1,2.

### 3 | RESULTS

#### 3.1 | Longitudinal trajectories of $A\beta$ -associated hippocampal subfield atrophy in NCI and MCI

There were significant  $A\beta$  and time interaction in ADNI-participants (NCI:  $\beta = -1.38$ ,  $p = .02$ ; MCI:  $\beta = -4.09$ ,  $p < .001$ ) and MACC MCI group ( $\beta = -2.88$ ,  $p = .05$ ), but not in MACC NCI group ( $p = .13$ ).

Regarding subfields, compared with the focal  $A\beta$ -related longitudinal volume decline in NCI, MCI exhibited more general involvement of subfields over time. Specifically, in ADNI MCI,  $A\beta$ -related

progressive atrophy widely spread to all the subfields ( $ps \leq .05$  after multiple comparison correction) (Figure 2, Table Se-2). For MACC MCI, we found longitudinal atrophy in the CA1 ( $\beta = -.50$ ,  $p = .014$ ), ML ( $\beta = -.53$ ,  $p = .027$ ), and the subiculum (trend-wise,  $\beta = -.38$ ,  $p = .051$ ; Figure 2, Table Se-2). Additionally, WMH matched MCI subsamples showed similar patterns for both datasets, with the MACC MCI subsample showing more robust  $A\beta$ -associated progressive atrophy in the same subfields compared with the whole MACC MCI sample, surviving multiple comparison correction (Table Se-3).

Regarding cognitively normal individuals, we found progressive volume decline in the CA1 ( $\beta = -.21$ ,  $p = .028$ ), CA4 ( $\beta = -.14$ ,  $p = .024$ ), HIP tail ( $\beta = -.34$ ,  $p = .027$ ), ML ( $\beta = -.25$ ,  $p = .018$ ), and GCL ( $\beta = -.16$ ,  $p = .023$ ) that were modulated by  $A\beta$  in ADNI NCI group (Figure 3, Table Se-4). In MACC NCI, we replicated the findings of  $A\beta$ -associated CA1 volume decline ( $\beta = -.55$ ,  $p = .046$ ; Figure 3, Table Se-4). None survived multiple comparison correction.

As a sanity check, we tested the time effects on hippocampal subfield atrophy. Unsurprisingly, all subfields showed longitudinal atrophy irrespective of  $A\beta$  burden in NCI and MCI for both ADNI and MACC datasets ( $ps \leq .05$  after multiple comparison correction, Table Se-5,6).

Controlling for age and gender, PET-MRI interval, and repeating analyses after excluding dementia converters and using global SUVR without PVC demonstrated largely similar results (Table Se-7,8). Due to the follow-up time difference between ADNI and MACC, exploratory analyses with the first 2-year follow-up data in the ADNI dataset revealed comparable results (Table Se-9).

Furthermore, the associations of  $A\beta$  with hippocampal subfield atrophy cross-sectionally were rather weak, which did not survive

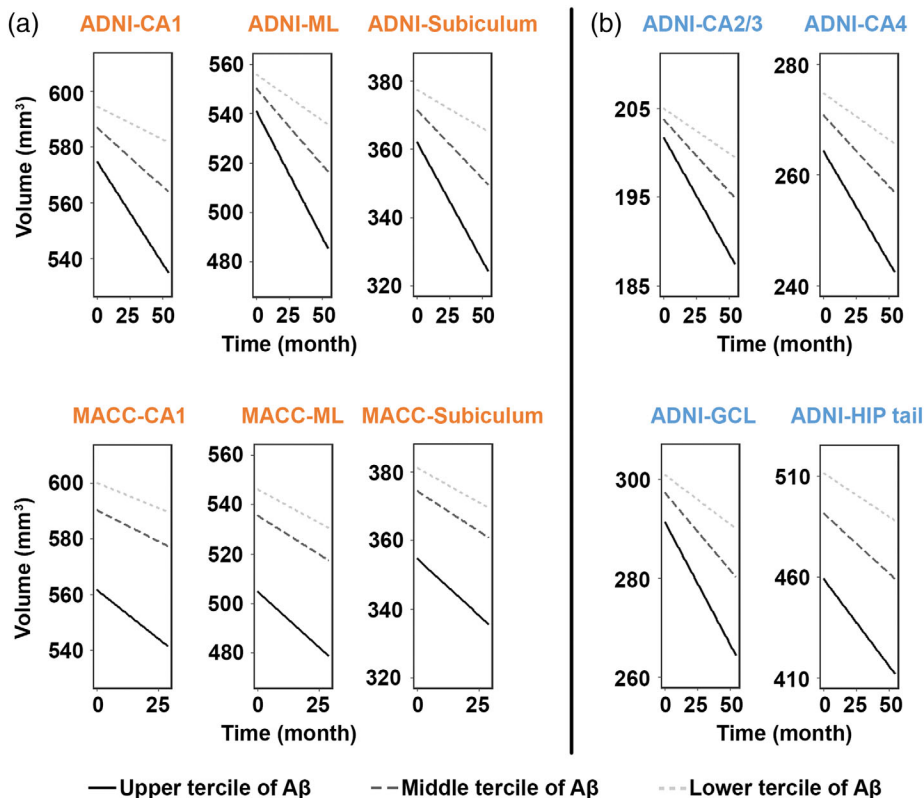


**FIGURE 2** Widespread progressive hippocampal subfield atrophy over time with greater  $A\beta$  burden in MCI across datasets. In ADNI dataset, higher level of  $A\beta$  correlated to faster decline in volume in all the seven hippocampal subfields, surviving Holm-Bonferroni multiple comparison correction. Similar patterns were observed in the CA1, ML, and subiculum (trend-wise,  $p = .051$ ) for the MACC dataset. Data were divided into three approximately equal-sized groups in terms of the log-transformed SUVR scores, represented by the solid line (upper tertile), dark gray dotted line (middle tertile), and the light gray dotted line (lower tertile). Hippocampal subfields in orange represented overlapping patterns (a), while those in blue represented distinct patterns between the two datasets (b). Abbreviations: GCL, Granule cell layer of the dentate gyrus; HIP tail, hippocampal tail; MCI, mild cognitive impairment; ML, molecular layer

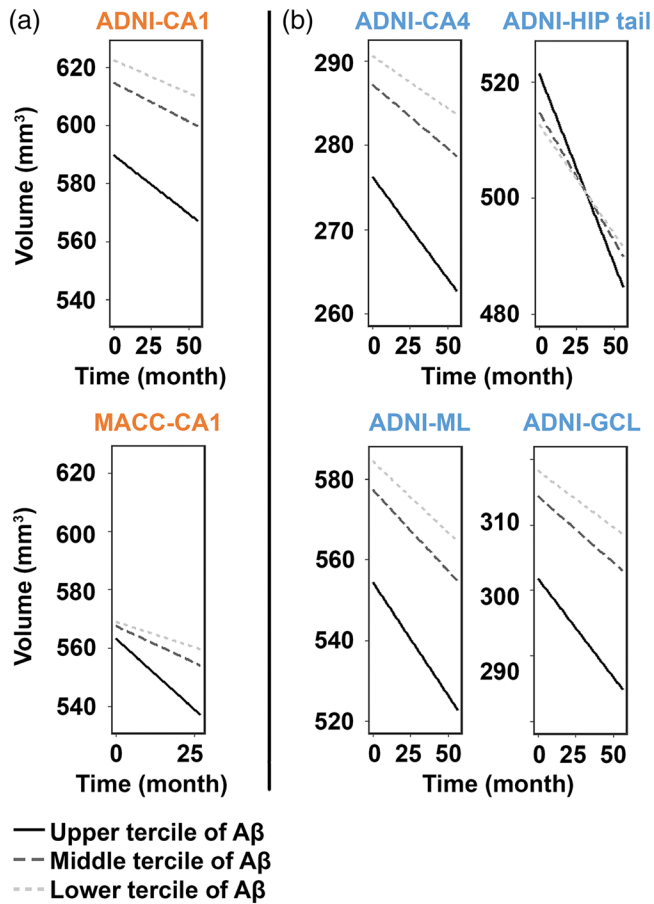


**FIGURE 3** Faster volume decline in the CA1 with greater A $\beta$  burden in NCI across datasets. Similar between the ADNI dataset and MACC dataset (denoted by orange color), higher level of A $\beta$  was associated with faster atrophy in the CA1 (a). Differently (denoted by blue color), NCI participants in the ADNI dataset also presented faster atrophy in the CA4, HIP tail, ML, and GCL (b). Data were divided into three approximately equal-sized groups in terms of the log-transformed SUVR scores, represented by the solid line (upper tertile), dark gray dotted line (middle tertile), and the light gray dotted line (lower tertile). Hippocampal subfields in orange represented overlapping patterns, while those in blue represented distinct patterns between the two datasets. None survived Holm–Bonferroni multiple comparison correction. Abbreviations: GCL, granule cell layer of the dentate gyrus; HIP tail, hippocampal tail; ML, molecular layer; NCI, no cognitive impairment

multiple comparison correction (Figure Se-1, 2). Also, as expected, MCI showed smaller subfield volume in all subfields than NCI cross-sectionally for both datasets (Table Se-10).

### 3.2 | Progressive hippocampal subfield atrophy correlated with memory decline in MCI

We found significant memory decline in MACC-participants (NCI:  $\beta = -.05$ ,  $p = .002$ ; MCI:  $\beta = -.03$ ,  $p = .003$ ), but not in ADNI-participants ( $ps > .05$ ). However, A $\beta$ -associated longitudinal subfield

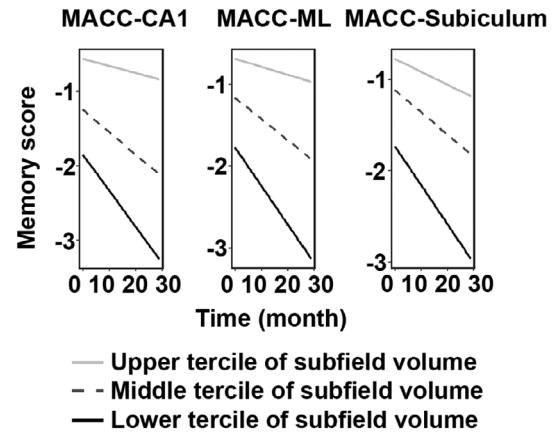


**FIGURE 4** Progressive hippocampal subfield atrophy was associated with faster memory decline over time in MACC MCI. For hippocampal subfields that showed progressive atrophy in association with A $\beta$ , faster decline in volume in these subfields correlated to faster memory decline in MCI for the MACC dataset, as well as ADNI dataset (described in text, and not shown in figure). All survived Holm–Bonferroni multiple comparison correction, except a trend-wise effect in the subiculum ( $p = .07$ ). Data were divided into three approximately equal-sized groups in terms of the hippocampal subfields volume, represented by the light gray solid line (upper tertile), dotted line (middle tertile), and the black solid line (lower tertile). Abbreviations: MCI, mild cognitive impairment; ML, molecular layer

atrophy was related to memory deterioration in MCI for both MACC (Figure 4;  $ps \leq .05$  for the CA1 and ML after multiple comparison correction) and ADNI ( $ps \leq .05$  after multiple comparison correction; Table Se-11), which was absent in NCI ( $ps > .05$ ).

Correlation between global A $\beta$  and memory decline in MCI was nonsignificant for both datasets ( $ps > .1$ ). Exploratory analyses showed region-specific associations between A $\beta$  in regions with early deposition (i.e., posterior cingulate cortex [PCC], precuneus, and medial orbital frontal gyrus; Palmqvist et al., 2017) and memory decline over time in MCI group of both datasets (Table Se-12). Such effects were also found between A $\beta$  in the precuneus and medial orbital frontal gyrus and memory decline in ADNI NCI group, but not in MACC NCI group due to the small sample size (Table Se-13).

## 4 | DISCUSSION

This study is the first demonstration of a longitudinal focal-to-widespread trajectory of hippocampal subfield atrophy in association with A $\beta$  over disease progression in nondemented elderly, replicated in two independent datasets. Compared with the subtle CA1 volume decline in NCI, MCI patients demonstrated more widespread subfield atrophy over time. Moreover, A $\beta$ -associated subfield atrophy rate was related to the rate of memory decline over time in MCI group. Our findings added novel knowledge on the association between A $\beta$  and neurodegeneration, and possible mechanisms of how A $\beta$  contributes to memory deterioration along disease progression prior to dementia.

#### 4.1 | Focal-to-widespread progressive hippocampal subfield atrophy over time with greater A $\beta$ burden in nondemented elderly

Importantly, both datasets consistently showed A $\beta$ -associated longitudinal atrophy progression in the CA1, ML, and subiculum. The CA1 and subiculum are key regions of the hippocampal circuit, being associated with input integration and memory retrieval, respectively (Small et al., 2011). Also, smaller ML has been correlated with poorer performance in memory retrieval (Zheng et al., 2018). Altogether, it may be implied that progressive atrophy in the CA1, ML, and subiculum relates to impaired memory functioning. That volume decline in these subfields correlated with memory decline in MCI lent further support.

Moreover, more widespread A $\beta$ -associated atrophy progression in ADNI MCI (versus MACC MCI) was not due to its longer follow-up (Table Se-9, ADNI 2-year longitudinal results), while it might be partly explained by cerebrovascular burden. Evidence has shown longitudinal hippocampal atrophy in association with baseline WMH before dementia (den Heijer et al., 2012), which has been suggested to be A $\beta$ -independent (Vemuri et al., 2015). Indeed, MACC MCI subsample after excluding those with more severe WMH showed A $\beta$ -associated volume decline in the same subfields, but to a stronger extent. Future studies need to investigate the relationship between A $\beta$ , individual cerebrovascular markers, and hippocampal subfield atrophy. In contrast to the observed widespread volume decline in MCI, NCI showed subtle volume decline in the CA1 selectively across both datasets. Interestingly, CA1 atrophy has also been observed in other disorders (e.g., bipolar disorder (Bearden et al., 2008), and schizophrenia (Ho et al., 2017)), suggesting a general CA1 vulnerability.

Taken together, we propose that A $\beta$ -associated subfield atrophy progression takes the form of a focal-to-widespread pattern as disease progresses from NCI to MCI. The AD Pathological Cascade model (Jack Jr. et al., 2013) and Amyloid/Tau/Neurodegeneration AD biomarkers system (Jack Jr. et al., 2016) have highlighted the role of individual AD biomarkers. Our results underscore the importance of associations between individual biomarkers, potentially leading to a better understanding of the underlying disease mechanism.

#### 4.2 | Possible underlying mechanisms of A $\beta$ modulation on the hippocampal subfield atrophy

Although the underlying neurotoxic mechanism of A $\beta$  remains controversial, it has been suggested that A $\beta$  induces synaptic loss and impairs neuronal function, resulting in neurodegeneration (Masters et al., 2006). Our study replicated previous findings of neocortex A $\beta$ -hippocampal atrophy association in nondemented elderly (Chetelat et al., 2010; Mormino et al., 2009). This could not be contributed to hippocampal A $\beta$  deposition (Chetelat et al., 2010), which is none or low in early stage (Thal, Rub, Orantes, & Braak, 2002). Several possibilities may be proposed. Specifically, key cortical regions for earliest A $\beta$  deposition (e.g., PCC/precuneus, orbital frontal; Palmqvist et al., 2017) could connect to hippocampus via white matter tracts

(e.g., from the orbital frontal via uncinate fasciculus, and from the PCC/retrosplenial via cingulum; Greicius, Supekar, Menon, & Dougherty, 2009; Vipin et al., 2019). This implies a structural pathway where abnormal A $\beta$  may modulate. Indeed, A $\beta$  has been associated with longitudinal impairment of white matter integrity before dementia (Vipin et al., 2019). Also, reduced precuneus-hippocampus functional connectivity has been found in nondemented participants with positive A $\beta$  compared with those with negative A $\beta$  (Sheline et al., 2010), providing a potential functional pathway. Notably, we showed that regional A $\beta$  burden in these regions was associated with memory decline especially in MCI patients (Table Se-12). We did not find global A $\beta$ -memory decline association, which was in line with previous animal/human literature (i.e., association between global A $\beta$  and cognition was generally absent or weak if any; Chetelat et al., 2012; Foley, Ammar, Lee, & Mitchell, 2015). Our findings may indicate a possible region-specific influence of A $\beta$  on longitudinal memory decline. Nonetheless, future work is needed to study the spatiotemporal relationship between regional A $\beta$ , hippocampal subfield degeneration, and memory decline in longer follow-up period. Another possibility links to soluble A $\beta$  that precedes A $\beta$  plaques formation, and has been suggested to affect hippocampal neurodegeneration via disturbing synaptic processing based on transgenic mice model of AD (Perez-Cruz et al., 2011). Soluble A $\beta$  has also been shown to induce hippocampal neuronal hyperactivity at early disease stage in transgenic AD mice, which has been hypothesized to be associated with neuronal dysfunction and cell death at a later stage (Busche et al., 2012; Busche & Konnerth, 2015).

Furthermore, given the association between tau deposition and atrophy in the whole hippocampus or hippocampal subfields (Apostolova et al., 2015), hippocampal subfield atrophy might be contributed by hippocampal tau deposition, which coincides with neocortex A $\beta$  accumulation in early stage (Braak, Alafuzoff, Arzberger, Kretschmar, & Del Tredici, 2006). Supporting preliminary evidence from ADNI MCI group suggested that A $\beta$ -associated progressive hippocampal subfield atrophy was more pronounced in MCI with p-tau positivity, but not in MCI with p-tau negativity (Table Se-14). Further systematic investigation into the interactions between region-specific tau and A $\beta$  deposition and their impact on neurodegeneration over time is needed using tau-PET method (Hall et al., 2017).

Regarding the selective CA1 volume decline in NCI, the CA1 has more than 21 types of inhibitory interneurons (Klausberger & Somogyi, 2008), and CA1 interneurons reduction has been found in transgenic AD mice (Takahashi et al., 2010). This might lead to an excitation-inhibition imbalance in the CA1, being associated with synaptic dysfunction and neuronal loss. The largest number of neurons (West & Gundersen, 1990) and capillaries (Lokkegaard, Nyengaard, & West, 2001) as estimated in the CA1 (vs. other subfields) might also contribute. Altogether, we propose that the CA1 atrophy represents a general and early vulnerability to AD and the atrophy spreads to other subfields over time via possible mechanisms as mentioned above. Although we could not pinpoint the exact neocortex A $\beta$ -hippocampal atrophy pathway(s), our result replications in two datasets provide convincing evidence for the focal-to-widespread pattern of A $\beta$ -associated subfield atrophy over time.

### 4.3 | Limitations and future directions

There were some limitations. Firstly, MACC-dataset had fewer NCI ( $n = 15$ ) than ADNI-dataset ( $n = 52$ ). However, similar results were observed between datasets. Secondly, other variables may also contribute to hippocampal subfield atrophy and disease progression (e.g., tau pathology and cerebrovascular factors) in addition to A $\beta$  (Apostolova et al., 2015; den Heijer et al., 2012). Future studies need to take into consideration the spatial quantification of A $\beta$  instead of an average A $\beta$  burden, and determine the contributing variables and the temporal relationships underlying disease progression. Finally, it would be interesting to test how A $\beta$  affects the hippocampus along the anterior–posterior axis in predementia stages.

## 5 | CONCLUSION

To conclude, converging results from two independent datasets showed that greater A $\beta$  burden correlated with selective CA1 volume decline in NCI and longitudinal atrophy extension into other subfields in MCI, resulting in a focal-to-widespread longitudinal trajectory. Moreover, the A $\beta$ -associated progressive subfield atrophy correlated with memory decline in MCI, hence, potentially serving as imaging markers for disease progression monitoring.

### ACKNOWLEDGMENTS

We thank all the participants for their contributions to the study. This research was funded by the National Medical Research Council (NMRC) Centre Grant (NMRC/CG/013/2013 and NMRC/CG/NUHS/2010 to Dr. Christopher Chen), the Biomedical Research Council, Singapore (BMRC 04/1/36/372 to Dr. Juan Zhou), the National Medical Research Council, Singapore (NMRC/CBRG/0088/2015, NMRC/CIRG/1390/2014 to Dr. Juan Zhou, and NMRC/CIRG/1446/2016 to Dr. Christopher Chen), and Duke-NUS Medical School Signature Research Program funded by Ministry of Health, Singapore. Dr. John T. O'Brien is supported by the NIHR Cambridge Biomedical Research Centre. The present study also received support from the Cambridge-NUHS Seed Funding (NUHSRO/2017/014/Cambridge/01) awarded to Dr. Christopher Chen and Dr. John T. O'Brien jointly.

Moreover, genuine acknowledgements should go to all researchers who involves in the data collection and sharing from the Alzheimer's Disease Neuroimaging Initiative (ADNI; <http://adni.loni.usc.edu/>). Data collection and sharing of ADNI for this project was funded by the ADNI (National Institutes of Health Grant U01 AG024904) and DOD ADNI (Department of Defense award number W81XWH-12-2-0012). ADNI is funded by the National Institute on Aging, the National Institute of Biomedical Imaging and Bioengineering, and through generous contributions from the following: AbbVie, Alzheimer's Association; Alzheimer's Drug Discovery Foundation; Araclon Biotech; BioClinica, Inc.; Biogen; Bristol-Myers Squibb Company; CereSpir, Inc.; Cogstate; Eisai Inc.; Elan Pharmaceuticals, Inc.; Eli Lilly and Company; EuroImmun; F. Hoffmann-La Roche Ltd and its affiliated company Genentech, Inc.; Fujirebio; GE Healthcare; IXICO Ltd.; Janssen Alzheimer

Immunotherapy Research & Development, LLC.; Johnson & Johnson Pharmaceutical Research & Development LLC.; Lumosity; Lundbeck; Merck & Co., Inc.; Meso Scale Diagnostics, LLC.; NeuroRx Research; Neurotrack Technologies; Novartis Pharmaceuticals Corporation; Pfizer Inc.; Piramal Imaging; Servier; Takeda Pharmaceutical Company; and Transition Therapeutics. ADNI clinical sites in Canada is receiving funds from the Canadian Institutes of Health Research. Private sector contributions are facilitated by the Foundation for the National Institutes of Health ([www.fnih.org](http://www.fnih.org)). The grantee organization is the Northern California Institute for Research and Education, and the study is coordinated by the Alzheimer's Therapeutic Research Institute at the University of Southern California. ADNI data are disseminated by the Laboratory for Neuro Imaging at the University of Southern California.

### CONFLICT OF INTEREST

Dr. John T. O'Brien reports grant from Avid/Lilly, personal fees from TauRx, Axon, Eisai, and GE Healthcare outside the submitted work. Other coauthors report no potential conflicts of interest.

### DATA AVAILABILITY STATEMENT

De-identified data are available upon requests from the corresponding authors.

### ORCID

Juan H. Zhou  <https://orcid.org/0000-0002-0180-8648>

### REFERENCES

- ADNI. (2011) ADNI 2 PET Technical Procedures Manual.
- ADNI. PET Pre-processing.
- Apostolova, L. G., Zarow, C., Biado, K., Hurtz, S., Boccardi, M., Somme, J., ... EADC-ADNI Working Group on the Harmonized Protocol for Manual Hippocampal Segmentation. (2015). Relationship between hippocampal atrophy and neuropathology markers: A 7T MRI validation study of the EADC-ADNI harmonized hippocampal Segmentation protocol. *Alzheimers Dement*, 11, 139–150.
- Bakker, A., Kirwan, C. B., Miller, M., & Stark, C. E. (2008). Pattern separation in the human hippocampal CA3 and dentate gyrus. *Science*, 319, 1640–1642.
- Barnes, J., Bartlett, J. W., van de Pol, L. A., Loy, C. T., Scahill, R. I., Frost, C., ... Fox, N. C. (2009). A meta-analysis of hippocampal atrophy rates in Alzheimer's disease. *Neurobiology of Aging*, 30, 1711–1723.
- Bearden, C. E., Thompson, P. M., Dutton, R. A., Frey, B. N., Peluso, M. A., Nicoletti, M., ... Soares, J. C. (2008). Three-dimensional mapping of hippocampal anatomy in unmedicated and lithium-treated patients with bipolar disorder. *Neuropsychopharmacology*, 33, 1229–1238.
- Becker, J. A., Hedden, T., Carmasin, J., Maye, J., Rentz, D. M., Putcha, D., ... Johnson, K. A. (2011). Amyloid-beta associated cortical thinning in clinically normal elderly. *Annals of Neurology*, 69, 1032–1042.
- Braak, H., Alafuzoff, I., Arzberger, T., Kretschmar, H., & Del Tredici, K. (2006). Staging of Alzheimer disease-associated neurofibrillary pathology using paraffin sections and immunocytochemistry. *Acta Neuropathologica*, 112, 389–404.
- Busche, M. A., Chen, X., Henning, H. A., Reichwald, J., Staufenbiel, M., Sakmann, B., & Konnerth, A. (2012). Critical role of soluble amyloid- $\beta$  for early hippocampal hyperactivity in a mouse model of Alzheimer's disease. *Proceedings of the National Academy of Sciences*, 109, 8740–8745.
- Busche, M. A., & Konnerth, A. (2015). Neuronal hyperactivity—A key defect in Alzheimer's disease? *BioEssays*, 37, 624–632.

- Chetelat, G., La Joie, R., Villain, N., Perrotin, A., de La Sayette, V., Eustache, F., & Vandenberghe, R. (2013). Amyloid imaging in cognitively normal individuals, at-risk populations and preclinical Alzheimer's disease. *NeuroImage: Clinical*, 2, 356–365.
- Chetelat, G., Villemagne, V. L., Bourgeat, P., Pike, K. E., Jones, G., Ames, D., ... Lifestyle Research, G. (2010). Relationship between atrophy and beta-amyloid deposition in Alzheimer disease. *Annals of Neurology*, 67, 317–324.
- Chetelat, G., Villemagne, V. L., Pike, K. E., Ellis, K. A., Ames, D., Masters, C. L., ... Australian Imaging, B., Lifestyle Study of Ageing Research, G. (2012). Relationship between memory performance and beta-amyloid deposition at different stages of Alzheimer's disease. *Neurodegenerative Diseases*, 10, 141–144.
- Chong, J. S. X., Liu, S., Loke, Y. M., Hilal, S., Ikram, M. K., Xu, X., ... Zhou, J. (2017). Influence of cerebrovascular disease on brain networks in prodromal and clinical Alzheimer's disease. *Brain*, 140, 3012–3022.
- Crane, P. K., Carle, A., Gibbons, L. E., Insel, P., Mackin, R. S., Gross, A., ... Alzheimer's Disease Neuroimaging Initiative. (2012). Development and assessment of a composite score for memory in the Alzheimer's Disease Neuroimaging Initiative (ADNI). *Brain Imaging and Behavior*, 6, 502–516.
- de Flores, R., La Joie, R., & Chetelat, G. (2015). Structural imaging of hippocampal subfields in healthy aging and Alzheimer's disease. *Neuroscience*, 309, 29–50.
- Delso, G., Furst, S., Jakoby, B., Ladebeck, R., Ganter, C., Nekolla, S. G., ... Ziegler, S. I. (2011). Performance measurements of the Siemens mMR integrated whole-body PET/MR scanner. *Journal of Nuclear Medicine*, 52, 1914–1922.
- den Heijer, T., van der Lijn, F., Ikram, A., Koudstaal, P. J., van der Lugt, A., Krestin, G. P., ... Breteler, M. M. (2012). Vascular risk factors, apolipoprotein E, and hippocampal decline on magnetic resonance imaging over a 10-year follow-up. *Alzheimer's Dement*, 8, 417–425.
- Fischl, B., Salat, D. H., Busa, E., Albert, M., Dieterich, M., Haselgrove, C., ... Dale, A. M. (2002). Whole brain segmentation: Automated labeling of neuroanatomical structures in the human brain. *Neuron*, 33, 341–355.
- Fischl, B., van der Kouwe, A., Destrieux, C., Halgren, E., Segonne, F., Salat, D. H., ... Dale, A. M. (2004). Automatically parcellating the human cerebral cortex. *Cerebral Cortex*, 14, 11–22.
- Foley, A. M., Ammar, Z. M., Lee, R. H., & Mitchell, C. S. (2015). Systematic review of the relationship between amyloid-beta levels and measures of transgenic mouse cognitive deficit in Alzheimer's disease. *Journal of Alzheimer's Disease*, 44, 787–795.
- Greicius, M. D., Supekar, K., Menon, V., & Dougherty, R. F. (2009). Resting-state functional connectivity reflects structural connectivity in the default mode network. *Cerebral Cortex*, 19, 72–78.
- Greve, D. N., Salat, D. H., Bowen, S. L., Izquierdo-Garcia, D., Schultz, A. P., Catana, C., ... Johnson, K. A. (2016). Different partial volume correction methods lead to different conclusions: An (18)F-FDG-PET study of aging. *NeuroImage*, 132, 334–343.
- Hall, B., Mak, E., Cervenka, S., Aigbirhio, F. I., Rowe, J. B., & O'Brien, J. T. (2017). In vivo tau PET imaging in dementia: Pathophysiology, radio-tracer quantification, and a systematic review of clinical findings. *Ageing Research Reviews*, 36, 50–63.
- Hanseeuw, B., Dricot, L., Lhommel, R., Quenon, L., & Ivanoiu, A. (2016). Patients with amyloid-negative mild cognitive impairment have cortical Hypometabolism but the hippocampus is preserved. *Journal of Alzheimer's Disease*, 53, 651–660.
- Ho, N. F., Iglesias, J. E., Sum, M. Y., Kuswanto, C. N., Sitoh, Y. Y., De Souza, J., ... Holt, D. J. (2017). Progression from selective to general involvement of hippocampal subfields in schizophrenia. *Molecular Psychiatry*, 22, 142–152.
- Hsu, P. J., Shou, H., Benzinger, T., Marcus, D., Durbin, T., Morris, J. C., & Sheline, Y. I. (2015). Amyloid burden in cognitively normal elderly is associated with preferential hippocampal subfield volume loss. *Journal of Alzheimer's Disease*, 45, 27–33.
- Iglesias, J. E., Augustinack, J. C., Nguyen, K., Player, C. M., Player, A., Wright, M., ... Alzheimer's Disease Neuroimaging Initiative. (2015). A computational atlas of the hippocampal formation using ex vivo, ultra-high resolution MRI: Application to adaptive segmentation of in vivo MRI. *NeuroImage*, 115, 117–137.
- Iglesias, J. E., Van Leemput, K., Augustinack, J., Insausti, R., Fischl, B., Reuter, M., & Alzheimer's Disease Neuroimaging Initiative. (2016). Bayesian longitudinal segmentation of hippocampal substructures in brain MRI using subject-specific atlases. *NeuroImage*, 141, 542–555.
- Jack, C. R., Jr., Bennett, D. A., Blennow, K., Carrillo, M. C., Feldman, H. H., Frisoni, G. B., ... Dubois, B. (2016). A/T/N: An unbiased descriptive classification scheme for Alzheimer disease biomarkers. *Neurology*, 87, 539–547.
- Jack, C. R., Jr., Knopman, D. S., Jagust, W. J., Petersen, R. C., Weiner, M. W., Aisen, P. S., ... Trojanowski, J. Q. (2013). Tracking pathological processes in Alzheimer's disease: An updated hypothetical model of dynamic biomarkers. *Lancet Neurology*, 12, 207–216.
- Ji, F., Pasternak, O., Liu, S., Loke, Y. M., Choo, B. L., Hilal, S., ... Zhou, J. (2017). Distinct white matter microstructural abnormalities and extracellular water increases relate to cognitive impairment in Alzheimer's disease with and without cerebrovascular disease. *Alzheimer's Research & Therapy*, 9, 63.
- Klausberger, T., & Somogyi, P. (2008). Neuronal diversity and temporal dynamics: The unity of hippocampal circuit operations. *Science*, 321, 53–57.
- La Joie, R., Perrotin, A., de La Sayette, V., Egret, S., Doeuve, L., Belliard, S., ... Chetelat, G. (2013). Hippocampal subfield volumetry in mild cognitive impairment, Alzheimer's disease and semantic dementia. *NeuroImage: Clinical*, 3, 155–162.
- Landau, S., Jagust, W. (2015) *Florbetapir processing methods*. 2014.
- Lokkegaard, A., Nyengaard, J. R., & West, M. J. (2001). Stereological estimates of number and length of capillaries in subdivisions of the human hippocampal region. *Hippocampus*, 11, 726–740.
- Masters, C. L., Cappai, R., Barnham, K. J., & Villemagne, V. L. (2006). Molecular mechanisms for Alzheimer's disease: Implications for neuroimaging and therapeutics. *Journal of Neurochemistry*, 97, 1700–1725.
- Mormino, E. C., Kluth, J. T., Madison, C. M., Rabinovici, G. D., Baker, S. L., Miller, B. L., ... Alzheimer's Disease Neuroimaging Initiative. (2009). Episodic memory loss is related to hippocampal-mediated beta-amyloid deposition in elderly subjects. *Brain*, 132, 1310–1323.
- Palmqvist, S., Scholl, M., Strandberg, O., Mattsson, N., Stomrud, E., Zetterberg, H., ... Hansson, O. (2017). Earliest accumulation of beta-amyloid occurs within the default-mode network and concurrently affects brain connectivity. *Nature Communications*, 8, 1214.
- Panin, V. Y., Kehren, F., Michel, C., & Casey, M. (2006). Fully 3-D PET reconstruction with system matrix derived from point source measurements. *IEEE Transactions on Medical Imaging*, 25, 907–921.
- Perez-Cruz, C., Nolte, M. W., van Gaalen, M. M., Rustay, N. R., Termont, A., Tanghe, A., ... Ebert, U. (2011). Reduced spine density in specific regions of CA1 pyramidal neurons in two transgenic mouse models of Alzheimer's disease. *The Journal of Neuroscience*, 31, 3926–3934.
- Reilhac, A., Merida, I., Itrace, Z., Stephenson, M. C., Weekes, A. A., Chen, C., ... Costes, N. (2018). Development of a dedicated Rebinner with rigid motion correction for the mMR PET/MR scanner, and validation in a large cohort of (11)C-PIB scans. *Journal of Nuclear Medicine*, 59, 1761–1767.
- Reuter, M., Rosas, H. D., & Fischl, B. (2010). Highly accurate inverse consistent registration: A robust approach. *NeuroImage*, 53, 1181–1196.
- Reuter, M., Schmansky, N. J., Rosas, H. D., & Fischl, B. (2012). Within-subject template estimation for unbiased longitudinal image analysis. *NeuroImage*, 61, 1402–1418.
- Sheline, Y. I., Raichle, M. E., Snyder, A. Z., Morris, J. C., Head, D., Wang, S., & Mintun, M. A. (2010). Amyloid plaques disrupt resting state default mode network connectivity in cognitively normal elderly. *Biological Psychiatry*, 67, 584–587.

- Small, S. A., Schobel, S. A., Buxton, R. B., Witter, M. P., & Barnes, C. A. (2011). A pathophysiological framework of hippocampal dysfunction in ageing and disease. *Nature Reviews. Neuroscience*, 12, 585–601.
- Takahashi, H., Brasnjevich, I., Rutten, B. P., Van Der Kolk, N., Perl, D. P., Bouras, C., ... Dickstein, D. L. (2010). Hippocampal interneuron loss in an APP/PS1 double mutant mouse and in Alzheimer's disease. *Brain Structure & Function*, 214, 145–160.
- Thal, D. R., Rub, U., Orantes, M., & Braak, H. (2002). Phases of a beta-deposition in the human brain and its relevance for the development of AD. *Neurology*, 58, 1791–1800.
- Vemuri, P., Lesnick, T. G., Przybelski, S. A., Knopman, D. S., Preboske, G. M., Kantarci, K., ... Jack, C. R., Jr. (2015). Vascular and amyloid pathologies are independent predictors of cognitive decline in normal elderly. *Brain*, 138, 761–771.
- Villemagne, V. L., Burnham, S., Bourgeat, P., Brown, B., Ellis, K. A., Salvado, O., ... Lifestyle Research, G. (2013). Amyloid beta deposition, neurodegeneration, and cognitive decline in sporadic Alzheimer's disease: A prospective cohort study. *Lancet Neurology*, 12, 357–367.
- Vipin, A., Loke, Y. M., Liu, S., Hilal, S., Shim, H. Y., Xu, X., ... Zhou, J. (2018). Cerebrovascular disease influences functional and structural network connectivity in patients with amnesic mild cognitive impairment and Alzheimer's disease. *Alzheimer's Research & Therapy*, 10, 82.
- Vipin, A., Ng, K. K., Ji, F., Shim, H. Y., Lim, J. K. W., Pasternak, O., ... Alzheimer's Disease Neuroimaging Initiative. (2019). Amyloid burden accelerates white matter degradation in cognitively normal elderly individuals. *Human Brain Mapping*, 40, 2065–2075.
- Weiner, M. W., Veitch, D. P., Aisen, P. S., Beckett, L. A., Cairns, N. J., Green, R. C., ... Alzheimer's Disease Neuroimaging Initiative. (2017). Recent publications from the Alzheimer's Disease Neuroimaging Initiative: Reviewing progress toward improved AD clinical trials. *Alzheimers Dement*, 13, e1–e85.
- West, M. J., & Gundersen, H. J. (1990). Unbiased stereological estimation of the number of neurons in the human hippocampus. *The Journal of Comparative Neurology*, 296, 1–22.
- Wisse, L. E., Biessels, G. J., & Geerlings, M. I. (2014). A critical appraisal of the hippocampal subfield segmentation package in FreeSurfer. *Frontiers in Aging Neuroscience*, 6, 261.
- Xu, X., Hilal, S., Collinson, S. L., Chong, E. J., Ikram, M. K., Venketasubramanian, N., & Chen, C. L. (2015). Association of magnetic resonance imaging markers of cerebrovascular disease burden and cognition. *Stroke*, 46, 2808–2814.
- Zheng, F., Cui, D., Zhang, L., Zhang, S., Zhao, Y., Liu, X., ... Qiu, J. (2018). The volume of hippocampal subfields in relation to decline of memory recall across the adult lifespan. *Frontiers in Aging Neuroscience*, 10, 320.

## SUPPORTING INFORMATION

Additional supporting information may be found online in the Supporting Information section at the end of this article.

**How to cite this article:** Zhang L, Mak E, Reilhac A, et al. Longitudinal trajectory of Amyloid-related hippocampal subfield atrophy in nondemented elderly. *Hum Brain Mapp.* 2020;1–11. <https://doi.org/10.1002/hbm.24928>